Linearized Recursive Least Square Methods for Real-Time Identification of Tire-Road Friction Coefficient

Mooryong Choi, Jiwon J. Oh , and Seibum B. Choi, *Member, IEEE*

***Abstract*—The tire-road friction coefficient is critical information for conventional vehicle safety control systems. Most previous studies in tire-road friction estimation have only considered either longitudinal or lateral vehicle dynamics which tends to cause significant underestimation of the actual tire-road friction coefficient. In this paper, the parameters, including the tire-road friction coefficient, of the combined longitudinal and lateral brushed tire model are identified by linearized recursive least square (LRLS) methods which efficiently utilize measurements related to both vehicle lateral and longitudinal dynamics in real time. Simulation study indicates that using the estimated vehicle states and the tire forces of the four wheels, the suggested algorithm not only quickly identifies the tire-road friction coefficient with a great accuracy and a robustness before tires reach their frictional limits but also successfully estimates the two different tire-road friction coefficients of the two sides of a vehicle on a split-μ surface. The developed algorithm was verified through vehicle dynamics software Carsim and Matlab/Simulink.**

***Index Terms*—Tire-road friction estimation, Nonlinear parameter identification, Recursive least square, Vehicle dynamics**

I. Introduction

THE IDENTIFICATION of peak tire-road friction coefficient is a critical task for guaranteeing the performances of many vehicle safety control systems such as anti-lock brake systems (ABS's), electronic stability programs (ESP's), and roll stability controls (RSC's) [1]–[8]. Several different approaches have been developed to identify the tire-road friction coefficient in real time. The methods presented in [9]–[12] are developed based on vehicle lateral dynamics. In [9], the tire-road friction coefficient and the cornering stiffness parameters are identified without requiring large slip angle with measurements from a differential GPS system and a gyroscope. In [10], the value of steering torque, which provides an earlier knowledge of the tire-road friction coefficient before tire forces saturate, is measured to identify the tire parameters. The algorithms in [13]–[18] use information related to vehicle longitudinal dynamics to design an identifier of the tire-road friction coefficient. In [17], each tire of a vehicle is taken into account individually for real-time estimation of the tire-road friction coefficient with various combinations of available sensor sets.

 The authors are with the Department of Mechanical Engineering, KAIST (Korea Advanced Institute of Science and Technology), Daejeon 305-701, Korea (e-mail: mucho@kaist.ac.kr; curoaura@kaist.ac.kr; sbchoi@kaist.ac.kr).

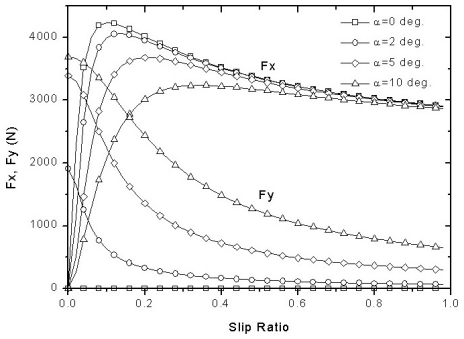

Fig. 1. Generic combined lateral and longitudinal tire force curves

However, since these methods only consider either longitudinal or lateral vehicle dynamics, the usage of these conventional tire-road friction coefficient identifiers is quite limited to certain conditions. Algorithms for the identification of the tire-road friction coefficient based only on longitudinal or lateral dynamics have to be carefully implemented for ESC or ABS, which are often activated in the situations that involve both longitudinal and lateral vehicle dynamics. By simply estimating longitudinal or lateral tire forces while braking in a turn, the vehicle stability control systems will significantly underestimate the actual tire-road friction coefficient because longitudinal tire force will decrease at a given slip ratio as the slip angle increases or lateral tire force decreases with a given slip angle as the slip ratio increases. Fig. 1 shows the phenomenon that lateral and longitudinal tire forces interact with each other. The underestimation of the actual tire-road friction coefficient can be followed by the deterioration of performance of the vehicle safety control systems.

Though the majority of tire-road friction coefficient algorithms is designed based on either vehicle lateral or longitudinal dynamics, only a small number of exceptions integrating both longitudinal and lateral vehicle dynamics for the tire-road friction identification are presented in [19]–[21]. In [19], longitudinal and lateral tire forces, and vehicle states are estimated by the extended Kalman filter. Then, Bayesian selection is applied for the identification of the tire-road friction coefficient using the estimated tire forces and vehicle states considering both longitudinal and lateral vehicle dynamics. However, this method cannot reflect changes of vehicle driving conditions, such as variations of tire pressure, wear, or tires since Bayesian selection requires preconstructed tire models with fixed tire paramerters. Because the mismatch

of the actual tire and the preconstructed tire models with fixed tire paramerters can cause huge errors in identifying the tire-road friction coefficient, the conventional usage of this method is quite difficult. In [20], a nonlinear observer that simultaneously estimates slip angles, tire forces, and tire-road friction coefficient is developed and evaluated. Though the performance of the suggested nonlinear observer in [20] is satisfactory, the logic requires a steering torque measurement which is not available for some commercial vehicles. Also, the nonlinear observer identifies only the tire-road friction coefficient among the several parameters of the combined slip brush model on which the nonlinear observer is based while the other parameters such as tread stiffness, which vary with tire age or pressure, are set to be known constants. Adopting the algorithm to a vehicle with tires that have different tire parameters can result in poor identification performance. The method presented in [21] also relies on a tire model with pre-identified tire parameters.

Unlike the works presented in [19]–[21], this paper focuses on the development of a tire-road friction coefficient identification algorithm that considers both vehicle lateral and longitudinal dynamics of individual wheels without pre-identified parameters for the tire model. The flow structure of the suggested algorithm is shown in Fig. 2. The tire forces estimator calculates lateral, longitudinal, and vertical tire forces using the readily available sensor signals on commercial vehicles including the steering wheel angle, the inertial measurements, the wheel speeds, and the engine and brake torques. The vehicle speeds estimator estimates the vehicle lateral and longitudinal speeds using the wheel speeds, the steering wheel angle, and the inertial measurements. The parameters of the combined longitudinal and lateral brushed tire model, including the tire-road friction coefficient, are identified in real time based on linearized recursive least square (LRLS) method utilizing the calculated slip angles, slip ratios, and corresponding lateral, longitudinal and vertical tire forces before the tire forces reach their frictional limits. After justifying the linearization of the nonlinear tire model by showing that the error due to the linear approximation is insignificant, the suggested algorithm based on LRLS was evaluated by two different simulations conducted on a μ-transient surface and a split-μ surface.

An important point that distinguishes the work of this paper from other methods in the literature is that the method to be introduced optimally utilizes the measurements related to longitudinal and lateral vehicle dynamics to identify the tire-road friction coefficient using four individual wheels in real time without pre-identified paramerters for the tire model.

II. Tire Model and Vehicle States Observer

The identifier of tire-road friction coefficient is developed based on an integrated longitudinal and lateral tire models. Several integrated longitudinal and lateral tire models are introduced in [22]. The structure of the tire model has to be simple enough to run it on an electronic control unit (ECU) of commercial vehicles in real time while reflecting tires' nonlinear characteristics including friction ellipse effect and

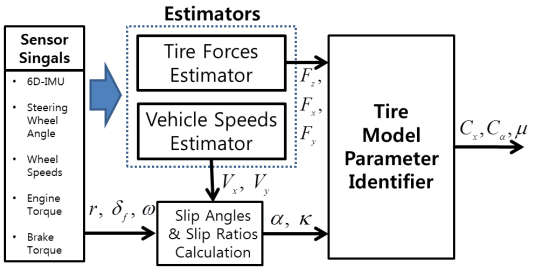

Fig. 2. Block diagram of tire-road friction estimation algorithm

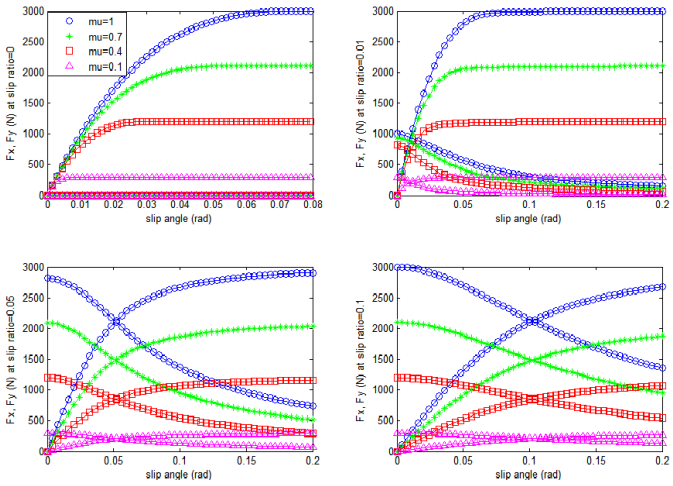

Fig. 3. Lateral and longitudinal forces versus slip angles with fixed slip ratios [0 0.01 0.05 0.1] on different surfaces

tire force saturation. Taking these aspects into consideration, the longitudinal and lateral combined brushed tire model [10] and [23] was chosen for the tire-road friction identifier and is presented as follows:

$$F_{x,i} = \frac{C_x\left(\frac{\kappa_i}{1+\kappa_i}\right)}{f_i}F_i \tag{1}$$

$$F_{y,i} = -\frac{C_\alpha\left(\frac{\tan\alpha_i}{1+\kappa_i}\right)}{f_i}F_i \tag{2}$$

where,

$$F_i = \begin{cases} f_i - \frac{1}{3\mu F_{z,i}}f_i^2 + \frac{1}{27\mu^2F_{z,i}^2}f_i^3 & \text{if } f_i \le 3\mu F_{z,i} \\ \mu F_{z,i} & \text{else} \end{cases}$$

$$f_i = \sqrt{C_x^2\left(\frac{\kappa_i}{1+\kappa_i}\right)^2 + C_\alpha^2\left(\frac{\tan\alpha_i}{1+\kappa_i}\right)^2}$$

$$\kappa_i = \frac{R_{e,i}\omega_i - V_{xt,i}}{V_{xt,i}} \tag{3}$$

$$\begin{bmatrix}\alpha_1\\ \alpha_2\\ \alpha_3\\ \alpha_4\end{bmatrix} = \begin{bmatrix}\delta_1\\ \delta_2\\ \delta_3\\ \delta_4\end{bmatrix} - \tan^{-1}\begin{bmatrix}\frac{V_y+l_f r}{V_x}\\ \frac{V_y+l_f r}{V_x}\\ \frac{V_y-l_r r}{V_x}\\ \frac{V_y-l_r r}{V_x}\end{bmatrix} \tag{4}$$

In (1) and (2), C_x, C_α, and μ are the tire longitudinal, lateral stiffness parameters, and the tire-road friction coefficient respectively. κ_i and α_i are the slip ratio and the slip angle of ith wheel as defined in (3) and (4), δ_i the steering angle, V_x the vehicle longitudinal speed, V_y the vehicle lateral speed, r the yaw rate, $R_{e,i}$ the tire effective radius, ω_i the wheel speed, and $V_{xt,i}$ the speed of a vehicle at the tire position along the steer angle where $i = 1,2,3,4$ which correspond to left front, right front, left rear and right rear wheel respectively. The reason for the longitudinal and lateral combined brushed tire model to be selected for the tire-road friction coefficient identifier is that it has just three parameters to be identified and fairly accurately describes the tire nonlinear characteristics such as friction ellipse effect and tire force saturation. Fig. 3 shows lateral and longitudinal forces versus slip angles at different fixed slip ratios and tire-road friction coefficients with constant vertical forces. It is noted that at the given slip ratios, the longitudinal forces decrease as the lateral forces increase along the value of slip angle. The longitudinal and lateral combined brushed tire model properly reflects tires nonlinear characteristics as shown in Fig. 3. The parameter identifier using LRLS is designed to find C_x, C_α, and μ with the estimated values of vertical forces $F_{z,i}$, the longitudinal tire forces $F_{x,i}$, the front lateral axle force $F_{y,f}$, the rear lateral axle force $F_{y,r}$, α_i and κ_i. To calculate α_i and κ_i, the vehicle states such as vehicle longitudinal speed, lateral speed and yaw rate are required.

The yaw rate can be measured using a gyro sensor which is readily available on commercial vehicles. However, sensors that measure vehicle lateral or longitudinal speeds are not very common for commercial vehicles due to their high costs. These values have to be estimated using other available signals. The vehicle state observer presented in [24] is integrated to estimate α_i and κ_i . The vehicle state observer with 6D-IMU signals in [24] which can handle the gravity corruption of accelerometers on banked or inclined roads shows a good performance both in severe and mild driving situations. $F_{z,i}$ are calculated using the method presented in [25]. Tire force estimators for finding values of $F_{x,i}$, $F_{y,f}$ and $F_{y,r}$ are illustrated in Section III.

III. Tire Force Estimation

A. Tire Force Estimator with Full Measurements

The estimated values of four longitudinal forces, and front and rear lateral axle forces are needed to identify the tire-road friction coefficient. Several methods which can estimate longitudinal and lateral tire forces simultaneously have been introduced in the literature. In [25], combined tire force estimation using the random-walk Kalman filter is introduced. However, this algorithm requires a derivative of sensor signal which needs a highly precise sensor. Though the tire force estimator in [19] shows satisfactory performance, the method causes a significant computational burden because the algorithm has to process the 21 by 21 matrices which corresponds to the state vector of the extended Kalman filter used in the tire force estimator. The tire force estimator developed in this paper which does not cause a huge computational burden or require derivations of sensor signals is based on Kalman filter using planar vehicle dynamics shown in Fig. 4.

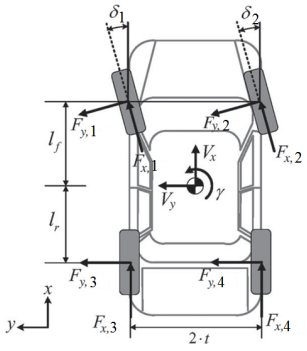

Fig. 4. Planar vehicle model

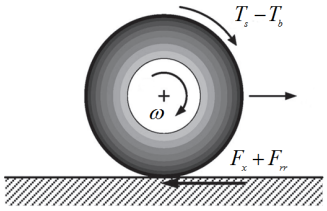

Fig. 5. Wheel dynamic model

The equation of motion for the planar vehicle shown in Fig. 4 is:

$$\begin{aligned} I_z\dot{r} &= l_f F_{y,f}\cos\left(\frac{\delta_1+\delta_2}{2}\right) - l_r F_{y,r}\cos\left(\frac{\delta_3+\delta_4}{2}\right) \\ &\quad + t\left(-F_{x,1}\cos\delta_1 + F_{x,2}\cos\delta_2 - F_{x,3}\cos\delta_3 + F_{x,4}\cos\delta_4\right) \\ &\quad + l_f F_{x,1}\sin\delta_1 + l_f F_{x,2}\sin\delta_2 - l_r F_{x,3}\sin\delta_3 - l_r F_{x,4}\sin\delta_4 \end{aligned} \tag{5}$$

I_z indicates the moment of inertia of the vehicle. l_f and l_r are the distances from the center of mass of the vehicle to the front axle and rear axle respectively. The equation of motion for the wheel shown in Fig. 5 is as follow:

$$I_w\dot{\omega}_i = T_{s,i} - R_e F_{x,i} - T_{b,i} - R_e F_{rr,i} \tag{6}$$

T_s and T_b are the shaft torque and the brake torque respectively. I_w is the moment of inertia of a wheel. F_{rr} is the rolling resistance force [26] can be obtained as follow:

$$F_{rr,i} = \mu_r F_{z,i} \tag{10}$$

μ_r is the rolling resistance coefficient.

The state for the Kalman filter is defined as follows:

$$\mathbf{x}(t) = [\mathbf{F} \quad \Omega \quad r]^T \tag{11}$$

where

$$\begin{aligned} \mathbf{F} &= \begin{bmatrix} F_{x,1} & F_{x,2} & F_{x,3} & F_{x,4} & F_{y,f} & F_{y,r} \end{bmatrix} \\ \Omega &= \begin{bmatrix} \omega_1 & \omega_2 & \omega_3 & \omega_4 \end{bmatrix} \end{aligned}$$

and

$$F_{y,f} = F_{y,1} + F_{y,2}, \quad F_{y,r} = F_{y,3} + F_{y,4}$$

The measurements are:

$$\mathbf{z}(t) = [a_x \quad a_y \quad r \quad \omega_1 \quad \omega_2 \quad \omega_3 \quad \omega_4]^T \tag{12}$$

$$A(t) = \left[\begin{array}{c|c} \mathbf{0}_{6\times 11} & \\ \hline -\frac{R_e}{I_w}\cdot \mathbf{I}_{4\times 4} & \mathbf{0}_{4\times 7} \\ \hline \frac{l_f\sin(\delta_1)-t\cos(\delta_1)}{I_z} \quad \frac{l_f\sin(\delta_2)+t\cos(\delta_2)}{I_z} \quad \frac{-l_r\sin(\delta_3)-t\cos(\delta_3)}{I_z} \quad \frac{-l_r\sin(\delta_4)+t\cos(\delta_4)}{I_z} \quad \frac{l_f\cos(\frac{\delta_1+\delta_2}{2})}{I_z} \quad \frac{-l_r\cos(\frac{\delta_3+\delta_4}{2})}{I_z} & \mathbf{0}_{1\times 5} \end{array}\right] \tag{7}$$

$$B(t) = \left[\begin{array}{c|cccc} \mathbf{0}_{1\times 6} & \frac{T_{b,1}+T_{s,1}-R_e\mu_r F_{z,1}}{I_w} & \frac{T_{b,2}+T_{s,2}-R_e\mu_r F_{z,2}}{I_w} & \frac{T_{b,3}+T_{s,3}-R_e\mu_r F_{z,3}}{I_w} & \frac{T_{b,4}+T_{s,4}-R_e\mu_r F_{z,4}}{I_w} & 0 \end{array}\right]^T \tag{8}$$

$$H(t) = \left[\begin{array}{cccccc|c} \cos(\delta_1) & \cos(\delta_2) & \cos(\delta_3) & \cos(\delta_4) & -\sin(\frac{\delta_1+\delta_2}{2}) & -\sin(\frac{\delta_3+\delta_4}{2}) & \mathbf{0}_{2\times 5} \\ \sin(\delta_1) & \sin(\delta_2) & \sin(\delta_3) & \sin(\delta_4) & \cos(\frac{\delta_1+\delta_2}{2}) & \cos(\frac{\delta_3+\delta_4}{2}) & \\ \hline \multicolumn{6}{c|}{\mathbf{0}_{5\times 6}} & \mathbf{I}_{5\times 5} \end{array}\right] \tag{9}$$

where

$$\begin{aligned} a_x &= \frac{1}{m}\left(F_{XF}+F_{XR}-F_{drag}\right) \\ a_y &= \frac{1}{m}\left(F_{YF}+F_{YR}\right) \end{aligned} \tag{13}$$

$$\begin{aligned} F_{XF} &= F_{x,1}\cos\delta_1 + F_{x,2}\cos\delta_2 - F_{y,1}\sin\delta_1 - F_{y,2}\sin\delta_2 \\ F_{XR} &= F_{x,3}\cos\delta_3 + F_{x,4}\cos\delta_4 - F_{y,3}\sin\delta_3 - F_{y,4}\sin\delta_4 \\ F_{YF} &= F_{x,1}\sin\delta_1 + F_{x,2}\sin\delta_2 + F_{y,1}\cos\delta_1 + F_{y,2}\cos\delta_2 \\ F_{YR} &= F_{x,3}\sin\delta_3 + F_{x,4}\sin\delta_4 + F_{y,3}\cos\delta_3 + F_{y,4}\cos\delta_4 \\ F_{drag} &= C_{av}V_x^2 \end{aligned}$$

F_{drag} is the aerodynamics drag force with the areodynamics coefficient, C_{av} [26]. Equations (6)-(13) are integrated to build the following state space system with the process noise $w(t)$ and the measurement noise $v(t)$:

$$\begin{aligned} \dot{\mathbf{x}}(t) &= A(t)\mathbf{x}(t) + B(t) + w(t) \\ \mathbf{z}(t) &= H(t)\mathbf{x}(t) + v(t) \end{aligned} \tag{14}$$

$A(t)$, $B(t)$ and $H(t)$ are defined in (7)-(9) whose $\mathbf{I_{i\times k}}$ and $\mathbf{0_{i\times k}}$ denote i by k identity matrix and zero matrix respectivley. Equation (14) is discretized using Zero-order hold for being applicable to the discrete-time Kalman filter [27] as follow:

$$\begin{aligned} \mathbf{x_{k+1}} &= A_k\mathbf{x_k} + B_k + w_k \\ \mathbf{z_k} &= H_k\mathbf{x_k} + v_k \end{aligned} \tag{15}$$

The algorithm of the discrete-time Kalman filter is:

$$\begin{aligned} \bar{x_{k+1}} &= A_k\hat{x}_k + B_k \\ M_{k+1} &= A_kP_kA_k^T + W_k \\ \hat{x}_k &= \bar{x_k} + P_kH_k^TV_k^{-1}(z_k - H_k\bar{x_k}) \\ P_k &= M_k - M_kH_k^T\left[H_kM_kH_k^T + V_k\right]^{-1}H_kM_k \end{aligned}$$

where W_k and V_k indicate the covariance matrices of w_k and v_k. The estimator includes the equation of motion for the planar vehicle but tire forces are considered to be unknown parameters to be estimated. These values are updated by the process noise w_k. The two front steer angles are basically from Ackerman steering geometry using the hand wheel steering input. The steer angles of the rear wheels are assumed to be zeros. For more details about Kalman filter, refer to [27].

B. Simplified Tire Force Estimator

For most driving situations when ABS or ESC are not activated, the following simplified estimator that does not require sensor signals of brake pressures or engine torque shows a sufficiently good performance. While accelerating, for most commercial vehicles, differential gear evenly distributes torque from engine into driving wheels on the left and right hand sides [26]. While braking, unless wheels are locked or ABS is activated, braking forces of front wheels and rear wheels have a certain ratio depending on disk size, proportioning valve and so on. Therefore, considering the characteristics of longitudinal tire forces mentioned above, four longitudinal tire forces can be expressed using the one variable, F_x as follows:

$$\text{During acceleration:} \qquad F_{x,1} = F_{x,2} = F_x \tag{16}$$

$$\text{During deceleration:} \qquad \begin{aligned} F_{x,1} &= F_{x,2} = K_sF_x \\ F_{x,3} &= F_{x,4} = (1-K_s)F_x \end{aligned} \tag{17}$$

In (16), a front wheel driving vehicle is assumed. For a rear wheel driving vehicle, (16) can be replaced with $F_{x,3} = F_{x,4} = F_x$. The gain K_s in the range of $(0.5, 1)$ in (17) can be expressed as a function of F_x since the proportioning valve that varies the brake pressure distribution between front wheels and rear wheels is depending on the master cylinder pressure which is proportional to F_x during mild driving. K_s can be set to be a constant for vehicles that are not equipped with proportioning valves. Therefore, the Kalman filter can be reconstructed with the following simplified states and measurements.

$$\begin{aligned} \mathbf{x}(t) &= \begin{bmatrix} F_x & F_{y,f} & F_{y,r} & r \end{bmatrix}^T \\ \mathbf{z}(t) &= \begin{bmatrix} a_x & a_y & r \end{bmatrix}^T \end{aligned}$$

$A(t)$, $B(t)$ and $H(t)$ in (14) are newly defined for the simplified tire force estimator as in (18)-(20).

Equations (5) and (13) are still integrated to build the state space system for the Kalman filter. However, since the wheel dynamics (6) are omitted in the simplified tire force estimator, four states related to wheel angular velocities and the measurements of shaft torques, brake torques, and four wheel angular velocities can be removed. As a result, overall computation for the tire force estimation greatly reduced and the tire force estimator became applicable to vehicles without

$$A(t) = \left[\begin{array}{cccc} \mathbf{0_{3\times 4}} & & & \\ \frac{l_f\sin(\delta_1)-t\cos(\delta_1)+l_f\sin(\delta_2)+t\cos(\delta_2)+K_s(-l_r\sin(\delta_3)-t\cos(\delta_3)-l_r\sin(\delta_4)+t\cos(\delta_4))}{I_z} & \frac{l_f\cos(\frac{\delta_1+\delta_2}{2})}{I_z} & \frac{-l_r\cos(\frac{\delta_3+\delta_4}{2})}{I_z} & 0 \end{array}\right] \quad (18)$$

$$B(t) = [\mathbf{0_{4\times 1}}] \quad (19)$$

$$H(t) = \left[\begin{array}{cccc} \cos(\delta_1)+\cos(\delta_2)+K_s(\cos(\delta_3)+\cos(\delta_4)) & -\sin(\frac{\delta_1+\delta_2}{2}) & -\sin(\frac{\delta_3+\delta_4}{2}) & 0 \\ \sin(\delta_1)+\sin(\delta_2)+K_s(\sin(\delta_3)+\sin(\delta_4)) & \cos(\frac{\delta_1+\delta_2}{2}) & \cos(\frac{\delta_3+\delta_4}{2}) & 0 \\ 0 & 0 & 0 & 1 \end{array}\right] \quad (20)$$

the shaft torque or brake pressure signals. However, the simplified tire force estimator is only valid when differential brake forces are not exerted by ABS or ESC and vehicle longitudinal dynamics is slow enough to neglect the wheel dynamics.

C. Simulation Results of Tire Force Estimators

The performances of the two tire force estimators were verified in the Carsim simulation whose result is presented in Fig. 6. Gaussian noises were added to the simulated measurements of a_x, a_y, ω_i and r to realistically recreate real application scenarios. The variances for the gaussian noises for a_x, a_y, ω_i, and r are $0.001m^2/s^4$, $0.001m^2/s^4$, $0.00028rad^2/s^2$ and $0.000001rad^2/s^2$. The values for the variances of the gaussian noises were determined based on the experimental data. The covariance matrix for the measurement noise is defined as follow:

$$V_k = \text{diag}\,[0.001 \quad 0.001 \quad 0.00028 \quad \ldots \quad 0.00028 \quad 0.000001]$$

The covariance matrix for the process noise is designed as follow:

$$W_k = \text{diag}[100 \quad \ldots \quad 100 \quad 1000 \quad 1000 \quad 0.00028 \quad \ldots \quad 0.00028 \quad 0.000001]$$

There are no huge differences between the estimation performances of the simplified and the full measurement tire force estimators without activations of ESC or ABS. However, as the ABS was initiated at around $t = 43$ s, the simplified tire force estimator was not able to track the actual tire forces properly due to the neglected wheel dynamics. The primary purpose of the tire-road friction coefficient identifier to be suggested is to figure out the tire-road friction coefficient in relatively mild driving situations when tires do not reach their frictional limits. Therefore, estimated tire forces by the simplified tire force estimator are expected to be reasonably correct for the use of the tire-road friction coefficient identifier in most cases. However, for a vehicle on a split-μ surface or when differential brakes forces are exerted, the use of the tire force estimator with full measurements is mandatory for guaranteeing the performance of the tire-road friction coefficient identifier. The simulation scenario involved both accelerating and braking in a turn on different road surfaces.

IV. Linearized Recursive Least Squares Methods with Adaptive Multiple Forgetting Factors

A. Linearized Recursive Least Square Method

The basic idea of least square methods is fitting a mathematical model to a sequence of observed data minimizing the sum of the squares of the difference between observed and computed data. By doing so, any noise or inaccuracies in the observed data are expected to have less effect on the accuracy of the mathematical model.

$$y(k) = \phi^T(k)\,\theta + v \quad (21)$$

$$V(\hat{\theta},k) = \frac{1}{2}\sum_{i=1}^{k}\lambda^{k-i}\left(y(i)-\phi(i)^T\hat{\theta}\right)^2 \quad (22)$$

The cost function $V(\hat{\theta},k)$ in (22) can be minimized by selecting proper parameters [28]. The minimizing parameters have the following closed form solution:

$$\hat{\theta}(k) = \left(\sum_{i=1}^{k}\left(\phi(i)\lambda^{k-i}\phi^T(i)\right)\right)^{-1}\sum_{i=1}^{k}\left(\phi(i)\lambda^{k-i}y(i)(i)\right)$$

However, solving the closed form solution every time whenever newly measured data is available is inefficient. To overcome this shortcoming, the recursive form is given as follows [28]:

$$\hat{\theta}(k) = \hat{\theta}(k-1) + L(k)\left(y(k)-\phi^T(i)\,\hat{\theta}(k-1)\right) \quad (23)$$

where

$$\begin{aligned} L(k) &= P(k)\,\phi(k) \\ &= P(k-1)\,\phi(k)\left(\lambda+\phi^T(k)\,P(k-1)\,\phi(k)\right)^{-1} \\ P(k) &= \left(I-L(k)\,\phi^T(k)\right)\lambda^{-1}P(k-1) \end{aligned} \quad (24)$$

$P(k)$ is referred to as the error covariance matrix. λ is a forgetting factor which will be explained in Section IV-B. This algorithm is valid only for linear systems. However, the brushed tire model is not only nonlinear but also impossible to lump the nonlinear terms that consist of parameters to be estimated and convert (1) and (2) into the linear form (21). Therefore, the following derivation is performed to extend the usage of the recursive least square (RLS) method to nonlinear systems [29].

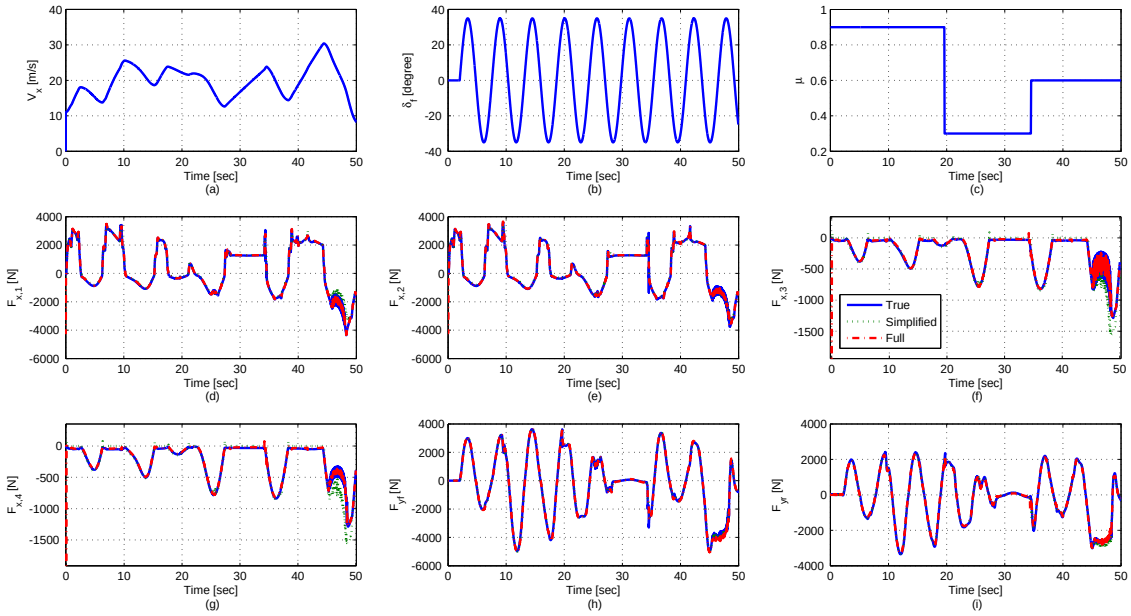

Fig. 6. Estimated tire forces. (a) Longitudinal speed profile. (b) steer angle profile (c) tire-road friction coefficient. (d) Front-left longitudinal tire force. (e) Front-right longitudinal tire force. (f) Rear-left longitudinal tire force. (g) Rear-right longitudinal tire force. (f) Front axle lateral tire force. (i) Rear axle lateral tire force.

$$y(k) = f(k,\theta)+v \tag{25}$$

$$V\left(\hat{\theta},k\right) = \frac{1}{2}\sum_{i=1}^{k}\lambda^{k-i}\left(y(i)-f\left(i,\hat{\theta}\right)\right)^2 \tag{26}$$

$y(k)$ can be approximated as follows:

$$y(k) \approx F(k)\left(\hat{\theta}(k)-\hat{\theta}(k-1)\right)+f\left(\hat{\theta}(k-1),k\right) \tag{27}$$

where

$$F(k) = \left.\frac{\partial f(\theta,k)}{\partial\theta}\right|_{\theta=\hat{\theta}(k-1)} \tag{28}$$

Define $z(k)$ as follow:

$$z(k) = y(k)+F(k)\left(\hat{\theta}(k-1)\right)-f\left(\hat{\theta}(k-1),k\right) \tag{29}$$

Substituting (27) into (29), the following linearized form is obtained.

$$z(k) \approx F(k)\,\hat{\theta}(k) \tag{30}$$

Since (30) has the exactly same form as (21), by replacing $\phi(k)$ and $y(k)$ in (23) with $F(k)$ and $z(k)$ respectively, the introduced RLS algorithm becomes applicable for nonlinear systems including the tire model (1) and (2). Equation (23) can also be modified:

$$\hat{\theta}(k) = \hat{\theta}(k-1)+L(k)\left(y(k)-f\left(\hat{\theta}(k-1),k\right)\right) \tag{31}$$

The parameters to be identified are defined as follow:

$$\theta(k) = \begin{bmatrix} C_x & C_\alpha & \mu \end{bmatrix}^T \tag{32}$$

$y(k)$ is updated whenever newly observed $F_{x,i}$, $F_{y,f}$ or $F_{y,r}$ from the tire force estimator are available. $F(k)$ is obtained by differentiating the tire model (1) and (2) with respect to $\theta(k-1)$ using the estimated values of $F_{z,i}$, α_i and κ_i which are obtained through the state estimator in [24]. At each time step, $F(k)$ is built with the newly estimated values. Though the tire-road friction coefficients for wheels on the left and right hand sides separately identified in V-B, at this state, with the assumption of equipping with the same tires for four wheels, the four tires share the same stiffness parameters C_α, C_x and tire-road friction coefficient μ because simultaneous identification of many parameters requires the excitation signal to be richer as the number of parameters to be identified increases. The comparison of identifying the three parameters and the four parameters, C_x, C_α, and μ's for the left and right hand sides of a vehicle are presented in V-B.

B. Adaptive multiple forgetting factors

The single forgetting factor λ in the range $(0,1]$ in (24) which gives more weight on lately measured data is usually set to be a constant. The procedure how the forgetting works in RLS is to multiply whole set of the previous (25) by the forgetting factor. For example, the n previous steps of (25) will be multiplied by the nth power of the forgetting factor in finding $\hat{\theta}$ which minimizes (26). However, updating the parameters that vary at different rates with a single forgetting factor can cause the wind-up problem [30]. Among the parameters to be identified, μ can vary abruptly as the road surface changes while the values of C_x and C_α which depend on tire properties such as tire size, tread width, tread stiffness, inflation pressure, load, and so on tend to be static for a short period time. Therefore, μ has to be assigned with a small value of forgetting factor to allow the sudden variation of the

TABLE I
FORGETTING FACTOR DESIGN PARAMETERS

Parameter	Value	Parameter	Value
γ_x	0.01	λ_α	0.9999
γ_y	0.01	λ_μ	0.9997
γ_μ	0.01	λ_1 and λ_2	0.999999
λ_κ	0.99997	ζ	0.7

parameter whereas forgetting factors close to unit values need to be allocated for C_x and C_α to prevent drastic changes of the estimated values of these parameters in the LRLS. To assign the parameters to be identified with different forgetting factors, vector-type forgetting is introduced [31] and [32]:

$$P(k) = \Lambda^{-1}\left(I - K(k)\phi^T(k)\right)P(k-1)\Lambda^{-1}$$

where

$$\Lambda = diag\left[\lambda_1, \lambda_2, \ldots, \lambda_n\right] \tag{33}$$

Instead of having the single forgetting factor in (24), the vector-type forgetting has a diagonal forgetting matrix Λ whose diagonal elements λ_j reflect the rate of the change of j^{th} parameter by scaling the error covariance matrix P.

While the forgetting factors for C_x and C_α, λ_1 and λ_2 respectively, are kept as constants, the forgetting factor for μ, λ_3 is set to vary depending on the side slip angle or the longitudinal slip ratio as follows:

$$\begin{aligned} &\text{Longitudinal forces available:} \quad \lambda_3 = \rho \cdot (\lambda_\kappa)^{\frac{\kappa_i(k)}{\gamma_x}} \\ &\text{Lateral forces available:} \quad \lambda_3 = \rho \cdot (\lambda_\alpha)^{\frac{\alpha_i(k)}{\gamma_y}} \end{aligned} \tag{34}$$

where

$$\rho = \begin{cases} \lambda_\mu^{\frac{\left(\frac{y(k)}{\mu F_z(k)} - \zeta\right)}{\gamma_\mu}} & \text{if} \quad \lambda_\mu^{\frac{\left(\frac{y(k)}{\mu F_z(k)} - \zeta\right)}{\gamma_\mu}} \leq 1 \\ 1 & \text{else} \end{cases} \tag{35}$$

In (34), as the slip angle or the slip ratio increases, the value of λ_3 will decrease which is followed by giving more weight to the data at bigger slip angle or slip ratio. The values of γ_x and γ_y are determined to scale the slip angle and the slip ratio as exponents of λ_κ, and λ_α , respectively, depending on the sampling time. In (35), ρ is designed to weigh the measurements as $y(k)$ approaches to $\mu F_z(k)$ which means the measurement has a rich information to identify μ. The value of ζ is set to be 0.7 so that the value of ρ decreases as the exponent of λ_μ, $\left(\frac{y(k)}{\mu F_z(k)} - \zeta\right)$, becomes positive when $y(k)$ is larger than 70% of $\mu F_z(k)$. The value of λ_μ to the power of $\left(\frac{y(k)}{\mu F_z(k)} - \zeta\right)$ scaled by γ_μ which also depends on the sampling time has the upper limit of a unit. The constant values of the design parameters, γ_x, γ_y, γ_μ, λ_κ, λ_α, λ_μ and ζ at the sampling time of 0.01 s are presented in Table I.

There are three reasons why the forgetting factors are chosen to vary depending on the value of slip angle or slip ratio. First, at a very low slip angle or slip ratio, it is extremely difficult to identify the tire-road friction coefficient as mentioned in [9]. This phenomenon can also be seen in Fig. 3. At the very tiny slip angle or ratio, the tire-road friction coefficient does not have much effect on tire forces. The gradients of curves of the tire force versus the slip ratio or the slip angle at this region remain the same regardless of the value of the tire-road friction coefficient. However, at the relatively large slip angle or ratio, tires start to show nonlinear characteristics which are early signs of tire force saturation which are directly related to the tire-road friction coefficient. Therefore, it is justifiable to weigh more on the data at the larger slip ratio or angle. Another reason of using the adaptive forgetting factor is that most vehicle state observers including the state observer used in this algorithm show a better accuracy when the vehicle slip or slip ratio is relatively large. This is because the persistent excitation condition [28] which most observers require is met with the large values of slip or ratio when the vehicle maneuver is comparably dynamic. Finally, signal to noise ratio (SNR) from the measurements such as accelerometers and gyro sensors is deteriorated at a very small slip angle or ratio. Therefore, it is reasonable to weigh more on data from more accurate vehicle states information by varying the forgetting factors.

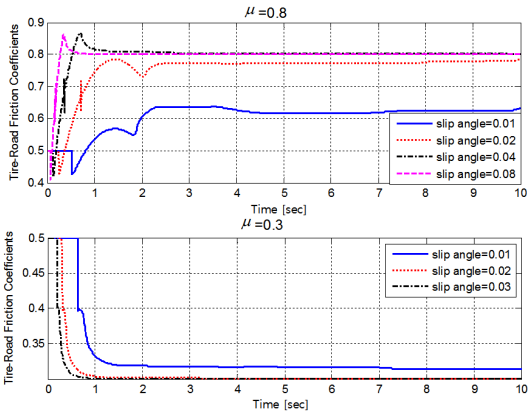

Fig. 7. Accuracy of friction coefficient identification at various slip angles on different surfaces

V. SIMULATION STUDY

The properties and performances of the proposed tire-road friction identification algorithm were investigated by simulations.

A. General Characteristics of Linearized RLS for Tire-Road Friction Estimation

First, to check the converging speed and the accuracy of the LRLS for tire-road friction coefficient identification at various magnitudes of slip angles, a simulation in an ideal situation was performed. In this simulation, tire forces are generated by the tire model (1) and (2) using sinusoids of $\alpha(t) = A\sin 3t$ with $A = 0.01,\ 0.02,\ 0.04,\ 0.08$ for the high μ surface with $\mu = 0.8$ and $A = 0.01,\ 0.02,\ 0.03$ for the low μ surface with $\mu = 0.3$. Gaussian noises were added to theses slip angles for the tire-road friction coefficient identifier with LRLS. F_z's are set to be constants. As mentioned in the previous section, the estimated value of tire-road friction coefficient took longer

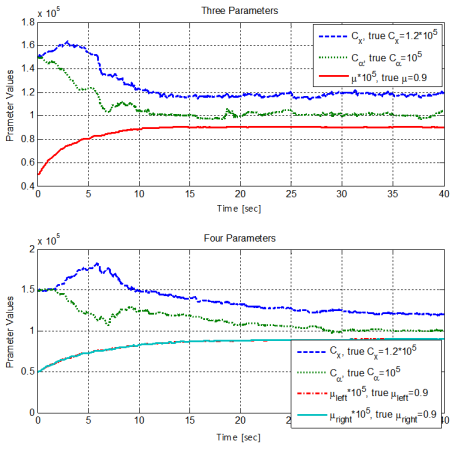

(a)

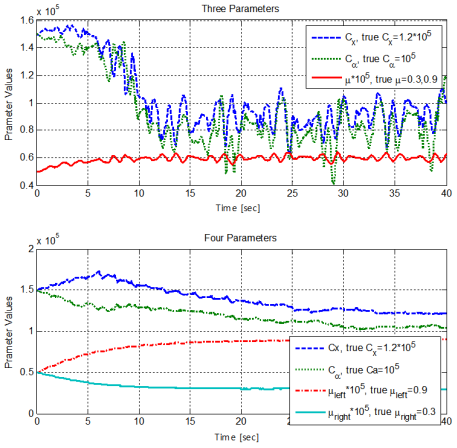

(b)

Fig. 8. Simulation results: Accuracy of friction coefficient identification depedning the number of parameters. (a) The same μ for the left and right hand side wheels . (b) The different μ's for the left and right hand side.

time to converge to its actual value at the small slip angles and the slip ratios as seen in Fig. 7. This is the natural characteristic of the tire-road friction coefficient identification using any tire models. Also, as shown in Fig. 7, the small slip angles or ratios are sufficient for identifying the low tire-road friction coefficient since tires show the nonlinear characteristic even with the small values of slip angles or ratios. The nonlinear characteristic is an early sign of tire saturation which depends on tire-road friction coefficient. For more details about these phenomena, [9] can be referred.

B. Comparison of identifying four parameters and three parameters

To successfully identify the two different tire-road friction coefficients of a vehicle on a split-μ surface, parameters to be identified are set to be as follows:

$$\theta(k) = \begin{bmatrix} C_x & C_\alpha & \mu_l & \mu_r \end{bmatrix}^T \tag{36}$$

μ_l and μ_r represent tire-road friction coefficients for the left and right hand side tires of a vehicle on a split-μ surface. The tire force estimator provides the values of four longitudinal tire forces corresponding to each wheel and the two lumped lateral

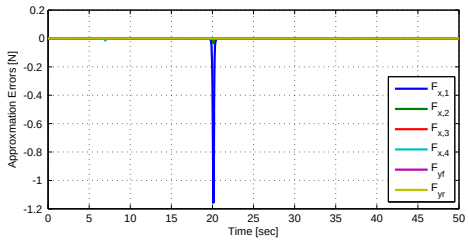

Fig. 9. Approximation errors.

forces for front and rear tires. When tires generate the lateral forces, the four parameters C_α, C_x, μ_l, and μ_r can be updated in the LRLS since the lumped lateral force is affected by the both left and right hand side tires. However, the longitudinal tire forces on the left hand side are irrelevant to the tire-road friction coefficient on the right side, μ_r and vice versa. Since there are the four parameters to be identified in (36), $P(k)$ and $F(k)$ in (23) and (28) become 4 by 4 and 4 by 1 respectively. However, the elements of $P(k)$ and $F(k)$ which correspond to μ_l or μ_r can be set to be zeros in the LRLS algorithm when the longitudinal tire forces of the opposite side update $y(k)$ in (29).

The simulation result in Fig. 8. compares the converging speeds of identifying the three parameters and the four parameters using the same simulation environments used in the previous subsection V-A with the input signals $\alpha(t) = 0.03\sin 2t$ and $\kappa(t) = 0.07\sin 3t$. Fig. 8(a) shows the identification of the four parameters took longer time to converge to their actual values due to the bigger number of parameters to be identified which eventually needs the excitation signals to be richer comparing to the signals required for the identification of the three parameters. However, as shown in Fig. 8(b), on a split-μ surface, the proposed method having three parameters to be identified could not properly distinguish the two different tire-friction coefficients of the left and right hand sides. The value of the tire-road friction coefficient identified using only the three parameters is somewhere between 0.3 and 0.9 which are true values of the tire-road friction coefficients of the left and right hand sides of the vehicle. Whereas, by assigning two different parameters, μ_l and μ_r for teh two sides of the vehicle on a split-μ surface, the proposed method successfully identifies the different tire-road friction coefficients. The proposed tire-road friction coefficient identifier in this paper uses three-parameter identification method for most driving situations. The four-parameter method is applied only when split-μ surface is detected by comparing the slip ratios of the left and right hand side wheels.

C. Analysis of adaptive multiple and single forgetting methods

To analyze the effectiveness of using the adaptive multiple forgetting factors over using a single forgetting factor, a simulation with slalom maneuvering with the steer angle profile in Fig. 6. at a constant speed, 85 km/h was performed. The simulation results of both using the single and the adaptive multiple forgetting methods are presented in Fig. 10. In this simulation, the lateral excitations were not large enough, in

other words, the tire forces are not fully saturated, to identify the unique tire parameters. As indicated in the plots of tire forces in Fig. 10, either using the single forgetting or the adaptive multiple forgetting, the errors between the observed tire forces and tire forces from the tire model (1) and (2) with the estimated parameters are insignificant while the values of the estimated parameters in case of using the single forgetting method converge to the wrong values. When tire forces do not reach their frictional limits, two different combinations of C_α and μ can generate almost the same lateral tire forces as seen in Fig. 10. However, one of the two combinations of the parameters is unrealistic since the value of μ converges to 1.3 while the values of μ for commercial vehicles do not exceed a unit. Therefore, by assigning different forgetting factors using the adaptive multiple forgetting method, the change rates for the values of C_x and C_α are kept to be relatively small because the values of C_x and C_α depend on intrinsic tire properties which do not vary abruptly so that the estimated parameters converge to their actual values.

D. Justification of the linearization of the nonlinear tire model

The nonlinear tire model (1) and (2) is linearized about the previously estimated $\hat{\theta}(k-1)$ with the currently estimated values of F_z's, α's and κ's to build $F(k)$ in (28) for running the LRLS algorithm (31). The linear approximation error has to be tolerable within the expected accuracy boundary to justify the linearization for the LRLS. The identification of the tire-road friction coefficient using the LRLS is supposed to be successful if the variation caused by the linearization of the nonlinear tire model (1) and (2) is within the expected ranges of uncertainty. The approximation error is defined as follows:

$$\begin{aligned}\varepsilon(k) = & f\left(\hat{\theta}(k)\right) - F(k)\left(\hat{\theta}(k) - \hat{\theta}(k-1)\right) \\ & - f\left(\hat{\theta}(k-1), k\right)\end{aligned} \tag{37}$$

Using the same simulation environment introduced in Section III-B, the approximation errors were calculated as shown in Fig. 9. The approximation error with $F_{x,1}$ had a stiff peak at around $t = 20$ s when the μ transition from 0.9 to 0.3 occurred. However, the value of the peak itself has an order of 10^0. Then, after several iterations, the order of the approximation errors decreased to 10^{-2}.

The absolute values of approximation errors are highly dependent on the sampling time because the longer sampling time causes the bigger deviations of the operating points from their linearized points. The simulation was performed at the sampling time of 0.01 s which is the slowest sampling rate of ECU's for commercial vehicles. With a shorter sampling time such as 0.005 s which is the typical sampling time for ECU's for commercial vehicles, the approximation errors can be bounded even in a smaller range. Since theses approximation errors are insignificant comparing to the errors of the estimated tire forces or vehicle states, the linearization of the nonlinear tire model (1) and (2) for RLS is justifiable.

VI. Simulation Results

The performance of the proposed algorithm was evaluated by simulations using the D-class sedan model in Carsim software. Two different simulations were performed on a μ-transient surface and a split-μ surface. The actual values of the parameters were found iteratively using a nonlinear solver.

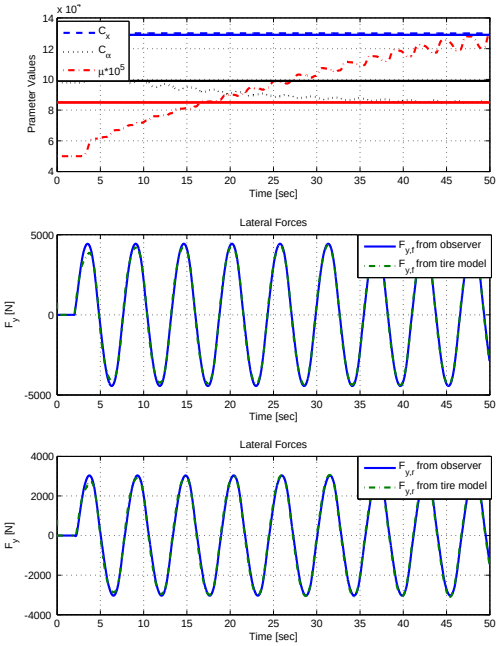

(a)

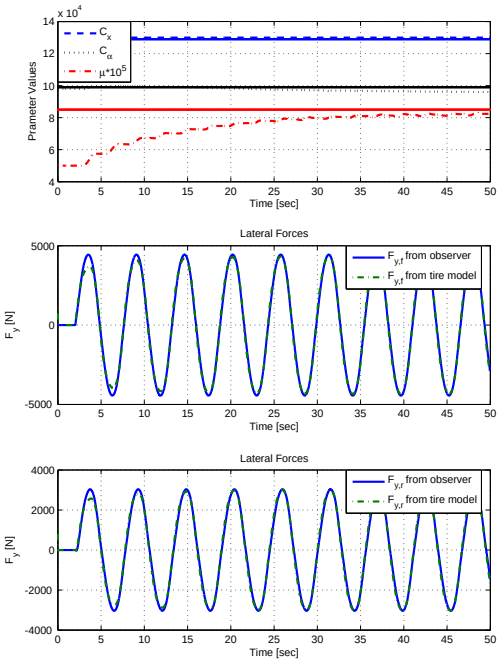

(b)

Fig. 10. Estimated parameters and tire forces using the tire model with the estimated parameters. (a) Single forgetting method . (b) Adaptive multiple forgetting method.

A. Simulation on a μ-transition surface

In the first simulation, the three parameters, C_x, C_α, and μ, were identified using the simplified tire force estimator on high, middle, and, low friction surfaces with the sensor signals which are readily available in commercial vehicles including

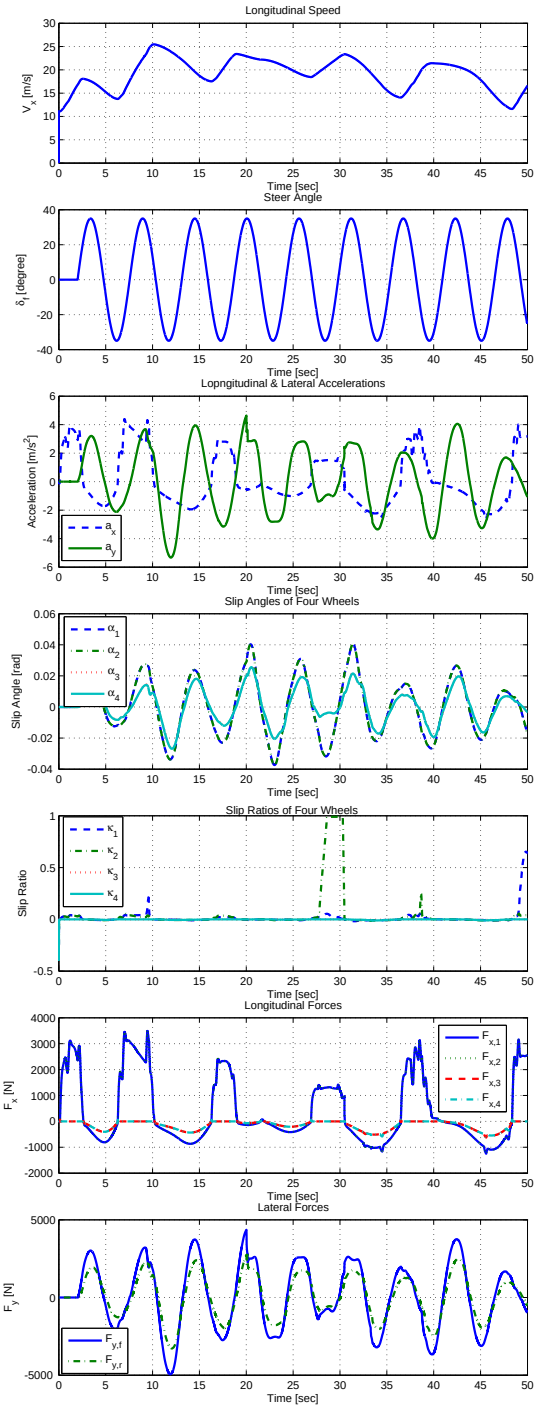

Fig. 11. Measured and observed signals of the first simulation.

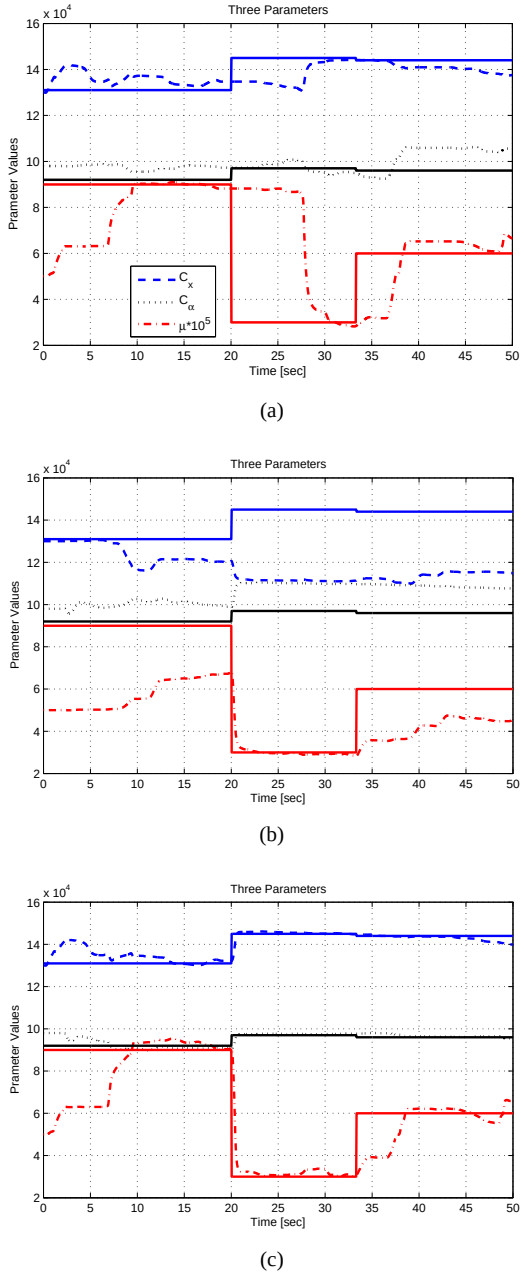

Fig. 12. Simulation results: Comparison of three estimators based on (a) Longitudinal dynamics only (b) Lateral dynamics only (c) Both longitudinal and lateral dynamics with corresponding true values (solid lines).

yaw rate, lateral and longitudinal accelerations and steer angle. The results of the first simulation are presented in Fig. 12. The first simulation was performed to evaluate the performance of the proposed tire-road friction identification algorithm with the measurements related to vehicle longitudinal dynamics only, vehicle lateral dynamics only and both vehicle longitudinal and lateral dynamics.

The sensor signals from Carsim and the observed values during the first simulation are plotted in Fig. 11. Fig. 12(a) and Fig. 12(b) show the estimation results using the measurements related to only longitudinal and lateral vehicle dynamics, respectively. Since longitudinal excitations alone was insufficient to identify the tire-road friction coefficient, there exists a huge delay of 7 s to 8 s in identifying μ transition from 0.9 to 0.3. In Fig. 12(b), the tire-road friction coefficient identifier underestimated the actual friction coefficient since the absolute values of lateral tire forces were not large enough comparing to the maximum lateral tire forces available on the surfaces where the vehicle located and the lateral forces at the given slip angles and the vertical loads were diminished along with the increasing longitudinal forces which is called the friction ellipse effect.

The estimation result presented in Fig. 12(c) which inte-

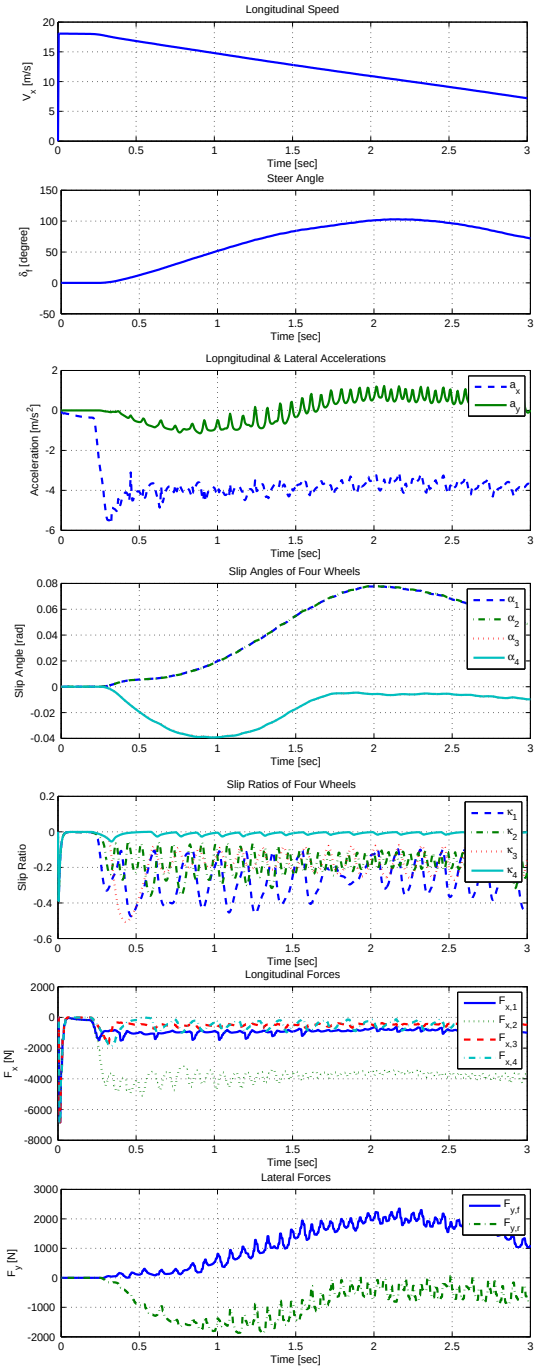

Fig. 13. Measured and observed signals of the second simulation.

grated measurements related to both lateral and longitudinal dynamics was satisfactory. The delays and lags of tracking actual parameter values were minimized while taking the friction ellipse effect into account.

B. Simulation on a split-μ surface

Four parameters, C_x, C_α, μ_l and μ_r, were identified in the second simulation to cope with the different values of friction coefficients on the left hand side and the right hand side of the vehicle on a split-μ surface. The tire force estimator with full measurements was integrated with the tire-road friction

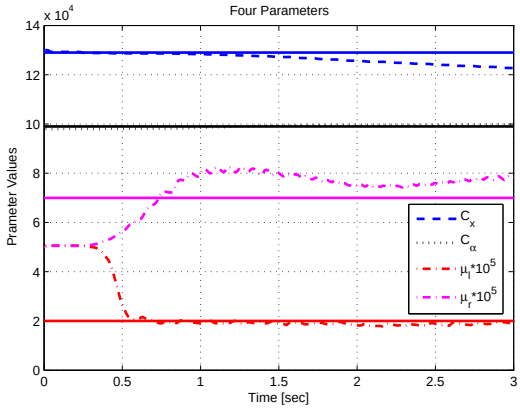

Fig. 14. Simulation result of the estimator on a split-μ surface with corresponding true values (solid lines).

identifier to handle the different longitudinal tire forces on the left hand side and the right hand side. The sensor signals from Carsim and the observed values during the second simulation are presented in Fig. 13.

A full braking was applied at around $t = 0.2$ s and the Carsim built-in ABS was initiated at around $t = 0.3$ s. It took longer time for the high μ parameter to converge to its actual value comparing to the low μ parameter because friction identification on a high μ surface requires more excitations as explained in Section V-A. The four-parameter identification successfully followed two different values of the friction coefficients of the split-μ surface. Overall performances of the friction identification algorithm was satisfactory though there were some minor errors which were caused by the mismatch of the actual and the used tire model, inaccuracies in the estimated values, and the noise of the measured signals.

VII. Conclusion

A new real-time tire-road friction coefficient identification algorithm which considers both lateral and longitudinal vehicle dynamics using only readily available sensor signals on commercial vehicles was developed and investigated in this paper. The proposed algorithm distinguishes itself from the previously reported methods by the following features: it can (i) detect two different tire-road friction coefficients of both sides of a vehicle on a split-μ surface, (ii) uses adaptive multiple forgetting factors based on slip angle and slip ratio in order to efficiently weigh meaningful measurements and (iii) identifies tire-road friction coefficient using the integrated lateral and longitudinal tire model without the pre-identified parameters to avoid underestimating the actual tire-road friction coefficient while fully utilizing longitudinal and lateral excitations.

The tire force estimator with full measurements is developed to take individual wheel dynamics into account using the readily available vehicle signals. Then, it is modified into the simplified tire force estimator to apply the friction estimation algorithm to the vehicles that do not have brake pressure sensors or engine torque signals. The simulation results using the developed tire force estimators prove that the proposed algorithm quickly estimates the tire-road friction coefficients

without requiring large slip angles or ratios on μ-transition and split-μ surfaces.

ACKNOWLEDGEMENTS

This work was supported by the National Research Foundation of Korea (NRF) grant funded by the Korea government (MEST), (No.2012-0000991) and the MSIP(Ministry of Science, ICT & Future Planning), Korea, under the C-ITRC(Convergence Information Technology Research Center) support program (NIPA-2013-H0401-13-1008) supervised by the NIPA(National IT Industry Promotion Agency).

REFERENCES

[1] C. Ahn, B. Kim, and M. Lee, "Modeling and control of an anti-lock brake and steering system for cooperative control on split-mu surfaces," *IJAT*, vol. 13, no. 4, pp. 571–581, 2012.
[2] K. Nam, H. Fujimoto, and Y. Hori, "Robust yaw stability control for electric vehicles based on active front steering control through a steer-by-wire system," *IJAT*, vol. 13, no. 7, pp. 1169–1176, 2012.
[3] M. H. Lee, K. S. Lee, H. G. Park, Y. C. Cha, D. J. Kim, B. Kim, S. Hong, and H. H. Chun, "Lateral controller design for an unmanned vehicle via kalman filtering," *IJAT*, vol. 13, no. 5, pp. 801–807, 2012.
[4] S. Kim, M. Tomizuka, and K. H. Cheng, "Smooth motion control of the adaptive cruise control system by a virtual lead vehicle," *IJAT*, vol. 13, no. 1, pp. 77–85, 2012.
[5] S. Kim, K. Park, H. Song, Y. Hwang, S. Moon, H. Ahn, and M. Tomizuka, "Development of control logic for hydraulic active roll control system," *IJAT*, vol. 13, no. 1, pp. 87–95, 2012.
[6] J. Song, "Integrated control of brake pressure and rear-wheel steering to improve lateral stability with fuzzy logic," *IJAT*, vol. 13, no. 4, pp. 563–570, 2012.
[7] R. Tchamna and I. Youn, "yaw rate and side-slip control considering vehicle longitudinal dynamics," *IJAT*, vol. 14, no. 1, pp. 53–60, 2013.
[8] M. H. Lee, K. S. Lee, H. G. Park, Y. C. Cha, D. J. Kim, B. Kim, S. Hong, and H. H. Chun, "Lateral controller design for an unmanned vehicle via kalman filtering," *IJAT*, vol. 13, no. 5, pp. 801–807, 2012.
[9] J. O. Hahn, R. Rajamani, and L. Alexander, "Gps-based real-time identification of tire-road friction coefficient," *IEEE Trans. Contr. Syst. Technol.*, vol. 10, no. 3, pp. 331–343, 2002.
[10] Y. Hsu, "Estimation and control of lateral tire forces using steering torque," Ph.D. dissertation, Stanford Univ., Stanford, CA, 2009.
[11] G. Yin, N. Chen, J. Wang, and J. Chen, "Robust control for 4ws vehicles considering a varying tire-road friction coefficient," *IJAT*, vol. 11, no. 1, pp. 33–40, 2010.
[12] C. Ahn, H. Peng, and H. E. Tseng, "Estimation of road friction for enhanced active safety systems: Dynamic approach," in *Proc. Amer. Contr. Conf.*, MO, USA, 2009.
[13] F.Gustafsson, "Monitoring tireroad friction using the wheel slip," *IEEE Control Syst. Mag.*, vol. 18, pp. 42–49, 1998.
[14] C. Lee, K. Hedrick, and Y. K, "Real-time slip-based estimation of maximum tireroad friction coefficient," *IEEE/ASME Trans. Mechatron.*, vol. 9, no. 2, 2004.
[15] H. Nishira, T. Kawabe, and S. Seiichi, "Road friction estimation using adaptive observer with periodical modification," in *Proc. IEEE Int.Conf. Contr. Applicat.*, Hwai'i, USA, 1999.
[16] F. Yu, K. Li, and J. Cao, "Nonlinear tire-road friction control based on tire model parameter identification," *IJAT*, vol. 13, no. 7, pp. 1077–1088, 2012.
[17] Y. Chen and J. Wang, "Adaptive vehicle speed control with input injections for longitudinal motion independent road frictional condition estimation," *IEEE Trans. Veh. Technol.*, vol. 60, no. 3, pp. 839–848, 2011.
[18] R. Rajamani, D. P. G. Phanomchoeng, and J. Lew, "Algorithms for real-time estimation of individual wheel tire-road friction coefficients," *IEEE/ASME Trans. Mechatron.*, vol. 17, no. 6, pp. 1183–1195, 2004.
[19] L. R. Ray, "Nonlinear tire force estimation and road friction identification: simulation and experiments," *Automatica*, vol. 33, no. 10, pp. 1819–1833, 1997.
[20] C. Ahn, H. Peng, and H. E. Tseng, "Robust estimation of road friction coefficient using lateral and longitudinal vehicle dynamics," *Veh. Syst. Dyn*, vol. 50, no. 6, pp. 961–985, 2012.
[21] L. Li, J. Song, H.-Z. Li, D.-S. Shan, L. Kong, and C. C. Yang, "Comprehensive prediction method of road friction for vehicle dynamics control," *Proc. of Inst. of Mech. Engineers, Part D*, vol. 223, no. 8, pp. 987–1002, 2009.
[22] L. Li, F.-Y. Wang, and Q. Zhou, "Integrated longitudinal and lateral tire/road friction modeling and monitoring for vehicle motion control," *IEEE Trans. Intell. Transport. Syst.*, vol. 7, no. 1, pp. 1–19, 2006.
[23] H. B. Pacejka, *Tire and Vehicle Dynamics*, 2nd ed. SAE, 2006.
[24] J. Oh and S. Choi, "Vehicle velocity observer design using 6d imu and multiple observer approach," *IEEE Trans. Intell. Transport. Syst.*, vol. 13, no. 4, pp. 1865–1879, 2012.
[25] W. Cho, J. Yoon, S. Yim, B. Koo, and K. Yi, "Estimation of tire forces for application to vehicle stability control," *IEEE Trans. Veh. Technol.*, vol. 59, no. 2, pp. 638–649, 2010.
[26] R. Rajamani, *Vehicle Dynamics and Control*. Springer, 2006.
[27] J. L. Speyer and W. H. Chung, *Stochastic Processes, Estimation, and Control*, 1st ed. SIAM, 2008.
[28] P. A. Ioannou and J. Sun, *Robust Adaptive Control*, 2nd ed. NJ: Prentice-Hall, 1996.
[29] P. J. G. Teunissen, *Dynamic Data Procssing: Recursive Least-Squares*. VSSD, 2001.
[30] A. Vahidi, A. Stefanopoulou, and H. Peng, "Recursive least squares with forgetting for online estimation of vehicle mass and road grade: Theory and experiments," *Veh. Syst. Dyn*, vol. 43, no. 1, pp. 31–55, 2005.
[31] S. Saelid, O. Egeland, and B. Foss, "A solution to the blow-up problem in adaptive controllers," *Modeling, Identi. and Cont.*, vol. 6, no. 1, pp. 36–39, 1985.
[32] S. Saelid and B. Foss, "Adaptive controllers with a vector variable forgetting factor," in *Proc. IEEE Int.Conf. Deci. and Contr.*, Kongsberg, Norway, 1983.

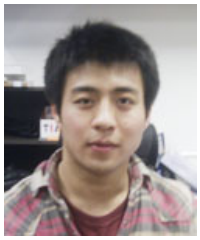

Mooryong Choi obtained his B.S. degree in mechanical engineering from Yonsei University, Seoul, Korea in 2008 and the M.S. degree in mechanical engineering from University of California, Los Angeles, in 2010. He is currently a Ph.D. candidate of mechanical engineering from Korea Advanced Institute of Science and Technology (KAIST). His research interests include vehicle dynamics, control and computer vision.

Jiwon Oh earned his B.S. degree and M.S. degree in mechanical engineering from Korea Advanced Institute of Science and Technology (KAIST). He is currently a researcher in automotive control laboratory of mechanical engineering department at KAIST. His research interests include vehicle state estimation and control.

Seibum B. Choi received B.S. degree in mechanical engineering from Seoul National University, Korea, M.S. degree in mechanical engineering from Korea Advanced Institute of Science and Technology (KAIST), Korea, and the Ph.D. degree in controls from the University of California, Berkeley in 1993. Since 2006, he has been with the faculty of the Mechanical Engineering department at KAIST. His research interests include fuel saving technology, vehicle dynamics and control, and active safety systems.